Chromosome Res (2011) 19:165–182
DOI 10.1007/s10577-010-9182-3

# Nuclei of chicken neurons in tissues and three-dimensional cell cultures are organized into distinct radial zones

**Doris Berchtold · Stephanie Fesser · Gesine Bachmann · Alexander Kaiser · John-Christian Eilert · Florian Frohns · Nicolas Sadoni · Joscha Muck · Elisabeth Kremmer · Dirk Eick · Paul G. Layer · Daniele Zink**

Received: 19 October 2010 / Revised: 22 December 2010 / Accepted: 22 December 2010 / Published online: 20 January 2011


**Abstract** We used chicken retinospheroids (RS) to study the nuclear architecture of vertebrate cells in a three-dimensional (3D) cell culture system. The results showed that the different neuronal cell types of RS displayed an extreme form of radial nuclear organization. Chromatin was arranged into distinct radial zones which became already visible after DAPI staining. The distinct zones were enriched in different chromatin modifications and in different types of chromosomes. Active isoforms of RNA polymerase II were depleted in the outermost zone. Also chromocenters and nucleoli were radially aligned in the nuclear interior. The splicing factor SC35 was enriched at the central zone and did not show the typical speckled pattern of distribution. Evaluation of neuronal and non-neuronal chicken tissues showed that the highly ordered form of radial nuclear organization was also present in neuronal chicken tissues. Furthermore, the data revealed that the neuron-specific nuclear organization was remodeled

Responsible Editor: Irina Solovei

**Electronic supplementary material** The online version of this article (doi:10.1007/s10577-010-9182-3) contains supplementary material, which is available to authorized users.

D. Berchtold · S. Fesser · A. Kaiser · N. Sadoni · J. Muck · D. Zink (✉)
Department Biologie II,
Ludwig-Maximilians-Universität (LMU)
München, Biozentrum,
Grosshadernerstr. 2,
82152 Planegg-Martinsried, Germany
e-mail: dzink@ibn.a-star.edu.sg

G. Bachmann · F. Frohns · P. G. Layer
Technische Universität Darmstadt, Fachbereich Biologie,
Schnittspahnstrasse 13,
64287 Darmstadt, Germany

J.-C. Eilert
BioImaging Zentrum,
Grosshadernerstr. 2,
82152 Planegg-Martinsried, Germany

E. Kremmer
Helmholtz Zentrum München,
Institut für Molekulare Immunologie,
Marchioninistr. 25,
81377 München, Germany

D. Eick
Helmholtz Zentrum München, Abteilung für Molekulare Epigenetik, Center of Integrated Protein Science,
Marchioninistr. 25,
81377 München, Germany

*Present Address:*
J. Muck · D. Zink
Institute of Bioengineering and Nanotechnology,
31 Biopolis Way, The Nanos, #04-01,
138669, Singapore

when cells spread on a flat substrate. Monolayer cultures of a chicken cell line did not show this extreme form of radial organization. Rather, such monolayer cultures displayed features of nuclear organization which have been described before for many different types of monolayer cells. The finding that an extreme form radial nuclear organization, which has not been described before, is present in RS and tissues, but not in cells spread on a flat substrate, suggests that it would be important to complement studies on nuclear architecture performed with monolayer cells by studies on 3D cell culture systems and tissues.

**Keywords** nuclear architecture · radial nuclear organization · 3D cell culture · retinospheroid · chicken neuron

**Abbreviations**

| | |
|---|---|
| DAPI | 4′,6′-diamidino-2′-phenylindole |
| 2D | Two-dimensional |
| 3D | Three-dimensional |
| E6 | Day 6 of embryonic development |
| FA | Formaldehyde |
| FISH | Fluorescence in situ hybridization |
| H4K8ac | Histone H4 acetylated at lysine 8 |
| PBS | Phosphate-buffered saline |
| PI | Propidium iodide |
| Pol II Ser 2 | RNA polymerase II phosphorylated at serine 2 |
| RS | Retinospheroid |
| TT | 0.2% Tween 20 and 0.2% Triton X-100 |

## Introduction

Three-dimensional (3D) in vitro cultures are of increasing importance for cell biological research. Adherent cells display profound structural and functional differences in in vitro cultures depending on whether they are organized into flat two-dimensional (2D) monolayers or into 3D tissue-like structures, respectively (Weaver et al. 1997; Cukierman et al. 2001; Rothermel and Layer 2001; Abbott 2003; Bissel et al. 2003; Wolf et al. 2003; Ghosh et al. 2005), and significant differences in gene expression patterns are observed between 2D and 3D cultures (Abbott 2003; Birgersdotter et al. 2005; Ghosh et al. 2005; Jacob et al. 2005). Whereas monolayer cells have been widely used to study the functional architecture of the cell nucleus, few studies have addressed nuclear organization and chromatin structure in 3D cell culture systems (Lelievre et al. 1998; Le Beyec et al. 2007; Meaburn and Misteli 2008; Lelievre 2009; Storch et al. 2010).

Here, we used retinospheroids (RS) to study nuclear architecture in a 3D cell culture model of the retina. RS are formed by embryonic chicken (*Gallus gallus*) retinal cells (Layer and Willbold 1993; Rothermel et al. 1997; Layer et al. 2002). The embryonic retinal cells differentiate in RS and after 10 days of in vitro culture the fractions of differentiated cells do not further increase (Rothermel and Layer 2001; Rothermel and Layer 2003). Cell differentiation in RS and corresponding changes in gene expression patterns depend on tissue architecture (Rothermel and Layer 2001; Jacob et al. 2005). Some of us demonstrated before that expression patterns of the different opsins came closest to the in vivo situation in RS kept at high serum (Jacob et al. 2005), which were also used here.

Here, we show that cells organized into RS display a highly ordered form of nuclear organization characterized by distinct radial zones. Cells from chicken neuronal tissue have a similar kind of nuclear organization. The special from of radial nuclear organization observed in RS and neuronal tissue was remodeled when cells spread on a flat substrate and was not present in monolayer cultures of a chicken cell line.

## Materials and methods

### Cell culture

The chicken HD12 macrophage cell line was kindly provided by Steffen Dietzel (LMU Munich). These cells were cultured as monolayers with RPMI 1640 medium supplemented with 10% fetal calf serum, 2% chicken serum, and penicillin/streptomycin. Metaphase spreads were prepared according to standard procedures (fixative: methanol/acetic acid 3/1).

### Preparation of chicken retinae and dorsal root ganglions and corresponding 2D and 3D in vitro cultures

Retinae were prepared from 6-day-old (E6, RS) or E13 (cultures on coverslips) chicken embryos (*G. gallus*, white leghorn). The procedure for the production of cultures on coverslips and of RS is described in detail in Rothermel and Layer (2001) and Jacob et al. (2005). RS were fixed after 10 days of in vitro culture. Dorsal root ganglions were prepared from E12 chicken embryos. Ganglions were either fixed immediately or were kept for 2 days in in vitro culture. Alternatively, cells were dissociated and seeded on coverslips. Dissociated cells were incubated for 2 days at 37°C and 5% $CO_2$ in DMEM F12 medium supplemented with 10% fetal calf serum, 25 ng/ml 7S nerve growth factor and antibiotics. Specimens were fixed with 4% formaldehyde buffered with phosphate-buffered saline (PBS) for 30 min (RS and dorsal root ganglions) or 10 min (coverslip cultures) at room temperature and stored in PBS. Nuclei were stained with 4,6-diamidino-2-phenyindole (DAPI, 0.5 μg/ml) or TO-PRO-3 iodide (1/4,000 in PBS; Molecular Probes, Leiden, The Netherlands) and mounted with Vectashield (Linaris, Wiesbaden, Germany).

### Chicken tissues

Chicken tissues were fixed for 36 h (adult brain) or 12 h (other tissues) with 4% formaldehyde buffered with PBS at 4°C, followed by extensive washing with PBS. Subsequently, brain tissue was incubated in 25% sucrose solution for 48 h and finally embedded into Neg 50 frozen section medium (Thermo Scientific, Germany) for the production of 8 μm thick cryosections. Other tissue was embedded into 4% agarose and 50 μm slices were cut with a vibratome.

### Staining with propidium iodide

RS were incubated for 1 h with PBS containing 0.5% Tween 20 and 0.5% Triton X-100 on a rotary mixer. Subsequently, RS were incubated on a mixer for 4 h with RNase A (5 μg/ml; Roche, Mannheim, Germany) at 37°C and were washed afterwards 3× with PBS-TT (TT: 0.2% Tween 20 and 0.2% Triton X-100). RS were then incubated on a mixer for 10 min with propidium iodide (PI; Molecular Probes, Leiden, The Netherlands) staining solution (0.25 μg/ml in PBS). Afterwards, they were washed 3× with PBS-TT and stained with DAPI.

### Fluorescence in situ hybridization

Labeled probes (pool of macrochromosomes 1–5 labeled with FITC or digoxigenin; pool of microchromosomes labeled with Cy3 or biotin) were obtained from Chrombios (Raubling, Germany) and provided in hybridization mix containing chicken Cot-1 DNA. The specificity of probes was tested by the supplier and by us using spreads of mitotic chromosomes from chicken DT 40 cells (data not shown). After denaturation (5 min at 75°C), probes were preannealed for 1.5–2 h at 37°C.

Preannealed FITC and Cy3-labeled probes were hybridized to methanol/acetic acid fixed specimens (chromosome spreads) for 3 days at 37°C. Previously, the fixed preparations were denatured (70% formamide, 0.6× SSC, 75°C, 2 min), dehydrated in a series of ice-cold ethanol (70%, 90%, and 100%), and air dried. After hybridization, slides were washed (5 min 4× SSC at room temperature, 5 min 2× SSC at 42°C, and 2× 5 min 0.1× SSC at 60°C), rinsed with PBS, stained with DAPI, and mounted with Vectashield (Linaris, Wiesbaden, Germany).

All incubations during the fluorescence in situ hybridization (FISH) procedure with RS were performed on a rotary mixer. Formaldehyde fixed RS were pretreated in the following way: RS were incubated for 15 min in PBS with 0.2% Tween 20 and 0.2% saponin and soaked for 1 h in 20% glycerol in PBS. Subsequently, they were frozen in liquid nitrogen and thawed and this was repeated three times. RS were washed for 5 min in SSC-TT (TT: 0.2% Tween 20 and 0.2% Triton X-100), incubated for 15 min in 0.1 M HCl, and washed again for 5 min in SSC-TT. Afterwards, RS were rinsed with 0.003% pepsin solution (in 0.01 M HCl) and digested in this solution for up to 10 min at 37°C. The reaction was stopped by rinsing in SSC-TT. RS were post-fixed with for 10 min with 1% formaldehyde in PBS and washed for 5 min in SSC-TT. Subsequently, they were incubated with RNase A for 2–3 h at 37°C. Afterwards, RS were washed in SSC-TT (3× 10 min), equilibrated for 15 min in 50% formamide/1× SSC, and incubated for 3–4 days at 37°C in this solution. Subsequently, they were denatured (70% formamide,

0.6× SSC, 8 min, 75°C), resuspended in the preannealed probe mix, and hybridized for 3 days at 37°C. Afterwards, RS were washed (10 min in 4× SSC-TT at room temperature and 10 min in 2× SSC at 42°C). When directly FITC and Cy3-labeled probes were used, RS were further washed twice with 0.1× SSC at 62°C, rinsed with 4× SSC-TT, and mounted with Vectashield after staining with DAPI.

When indirectly labeled probes were used, RS were further washed only once with 0.1× SSC at 62°C and incubated for 2 h with blocking solution (PBS with 5% bovine serum albumin, 0.5% Triton X-100 and 0.5% Tween 20). Fluorochrome-conjugated avidin and a fluorochrome-conjugated anti-digoxigenin antibody (Roche, Mannheim, Germany) were diluted in blocking solution and RS were incubated with this solution for at least 6 h. Afterwards, RS were washed 4× for 10 min in PBS-TT and mounted after staining with DAPI.

## Immunostaining

The procedure for the immunostaining of monolayer cells was performed as described (Sadoni et al. 1999). RS were blocked for 2 h (blocking solution: see "Fluorescence in situ hybridization" section) and incubated for at least 12 h with the primary antibody diluted in blocking solution. Subsequently, they were washed four times for 20 min with PBS-TT and incubated for at least 6 h with the secondary antibody diluted in blocking solution. After washing (4× 20 min with PBS-TT), the DNA was stained with DAPI and specimens were mounted with Vectashield. The following primary antibodies and antisera were used: mouse anti-SC35 (Sigma-Aldrich, Schnelldorf, Germany), mouse anti-H3K27me3 (histone H3 trimethylated at lysine 27; Abcam, Cambridge, UK), mouse anti-fibrillarin (Abcam, Cambridge, UK), rabbit anti-H4K8ac (histone H4 acetylated at lysine 8; R232/8, kindly provided by Bryan M. Turner, Univ. of Birmingham, UK), rabbit anti-H3K9me2 (histone H3 di-methylated at lysine 9) conjugated with biotin (Biomol, Hamburg, Germany), mouse anti-actin (Santa Cruz, Heidelberg, Germany), rabbit anti-β3 tubulin (Chemicon, Hampshire, UK), mouse anti-vimentin (Abcam, Cambridge, UK), rabbit anti-calretinin (Abcam, Cambridge, UK), and human CREST autoimmune serum (Immunovision Springdale, USA). In addition, the mouse Rho4D2 antibody specific for rods (generous gift from D. Hicks, Strasbourg, France) and the rabbit CERN906 antibody specific for red and green opsins (generous gift of Willem DeGrip, University of Nijmegen, The Netherlands) were used, as well as a mouse antibody against acetylcholinesterase (generous gift of Karl Tsim, Hongkong) and a rabbit anti-calretinin antibody (Swant, Bellinzona, Switzerland). Furthermore, two antibodies against the active form of RNA Pol II were used. mAbs against phosphorylated forms of either serine 2 (CTD-7-3E10) and serine 5 (CTD-4-3E8) of the C-terminal domain of Pol II were generated by using the following peptides coupled to ovalbumin (H. R. Rackwitz, Peptide Speciality Laboratories GmbH, Heidelberg, Germany): for phospho-serine 2, YSPTSPSYS(phospho)PTSPS; for phospho-serine 5, YSPTS(phospho)PSYSPTSPS. Both antibodies recognize only the Pol IIO form in immunoblots and do not bind to the unphosphorylated peptide in ELISA. The mAb CTD-7-3E10 has the subclass IgG1, the mAb CTD-4-3E8 the subclass IgG2a. Hybridoma and supernatants were tested as described previously (Chapman et al. 2007).

All secondary antibodies used were raised in goat. The following antibodies obtained from Dianova (Hamburg, Germany) were applied: anti-rabbit FITC- or Cy3-conjugated, anti-mouse TRITC, anti-human Cy3, and anti-rat FITC- or Cy3-conjugated. An anti-mouse and an anti-rabbit antibody both conjugated with Alexa-488 were obtained from Invitrogen (Karlsruhe, Germany).

## Microscopy

Epifluorescence microscopy of methanol/acetic acid fixed metaphase spreads was performed with a Zeiss Axiovert 135 TV fluorescence microscope equipped with a CCD camera (MicroMax, Princeton Instruments, USA). DAPI-stained chicken brain sections were imaged with an Axio Observer D1 microscope (Carl Zeiss, Oberkochen, Germany) equipped for epifluorescence. All other specimens were imaged by confocal laser scanning microscopy using either a TCS SP or a TCS SP2 AOBS microscope (Leica, Bensheim, Germany). In both cases, an HCX 63×/1.4 Plan-Apochromat oil immersion objective was used and both microscopes were equipped with an argon laser (488 nm), a DPSS laser (561 nm), and a helium–neon laser (633 nm). In addition, the TCS SP2 AOBS microscope was equipped with a diode laser (405 nm), which was used for DAPI imaging. The pixel size was adjusted to 100×100 nm ($x$, $y$) and the axial distance

between light optical sections was 250 nm in cases where individual nuclei were scanned in detail.

### Software

The following software was used for imaging, fluorescence intensity profiles and the arrangement of images: Metamorph (4.5, Visitron, Puchheim, Germany), LCS (Leica, Bensheim, Germany), Image J (http://rsb.info.nih.gov/ij/), and Adobe Photoshop 7.0.

## Results

### Overall organization of chromatin and nucleoli in RS nuclei

First, we addressed the overall organization of chromatin in RS nuclei. Staining of chromatin with DAPI resulted in a characteristic pattern (Fig. 1a, b, g), which was similar in all RS nuclei examined (several thousand nuclei from about 200 RS examined in the

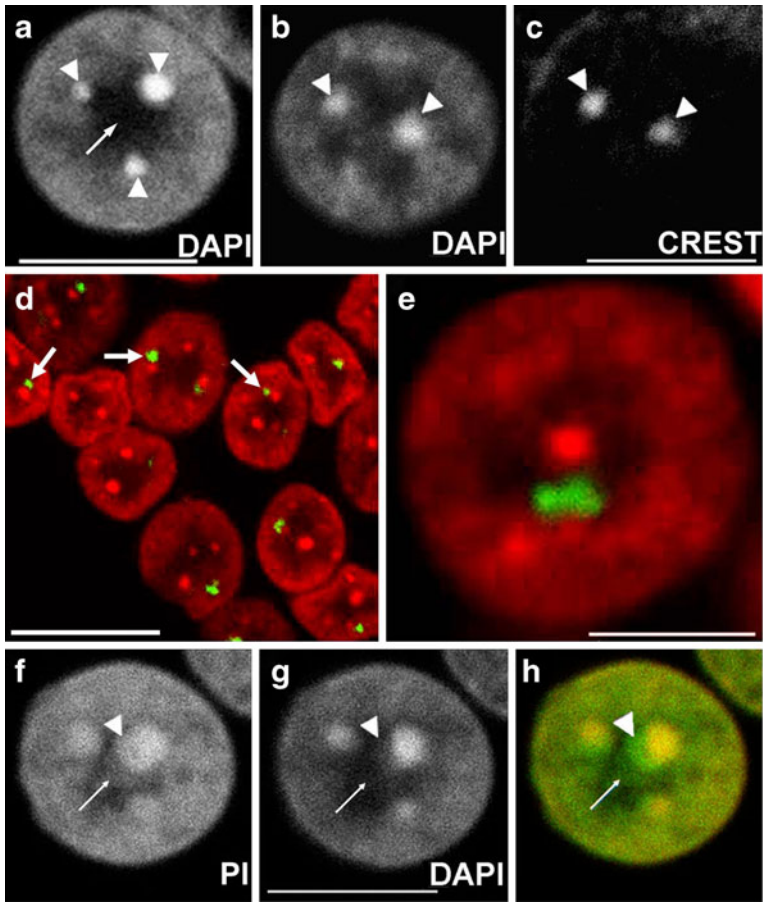


**Fig. 1** Overall organization of chromatin and nucleoli in RS nuclei. The panels show single light optical sections. **a**, **b** DAPI fluorescence. **a** The *arrow* indicates the central DAPI-depleted zone. Chromocenters (*arrowheads*) intensely stained by DAPI are aligned along the border between the central DAPI-depleted and the peripheral DAPI-positive zone. **b**, **c** Show the same nuclear plane. Chromocenters (*arrowheads*) were stained by CREST antiserum (**c**). **d** Field of nuclei (DAPI *red*; false colors are used) after immunostaining of fibrillarin (*green*). Nucleoli (*green*) are aligned along the boundary between the DAPI-depleted and the DAPI-positive zones and are frequently associated with chromocenters (*arrows*). **e** Shows nucleoli (*green*; DAPI *red*) not enclosed by perinucleolar heterochromatin exposed to the central DAPI-depleted zone. The nuclear plane displayed was relatively close to the upper boundary of the DAPI-depleted zone and therefore a chromocenter associated with this boundary appears to locate in the center of this zone. **f**, **g** Show the same plane and display either the propidium iodide (**f**) or the DAPI (**g**) staining pattern. The central zone devoid of DAPI staining displays PI staining (*arrow*), although the staining intensity is relatively weak. Particularly intense PI staining is present in regions close to chromocenters (*arrowheads*) devoid of DAPI staining. **h** Shows the merge of **f** and **g**. DAPI is shown in *red* and PI in *green*. *Scale bars* 5 μm (**a**, **c**, **e**, **g**) and 10 μm (**d**)

course of this study; >50 DAPI-stained nuclei are shown in Figs. 1, 2, 3, 4, 5, and 6). The nuclei displayed a peripheral zone enriched in chromatin that was clearly stained by DAPI (DAPI-positive zone) and a central region that was only faintly stained (DAPI-depleted zone). The peripheral DAPI-positive zone was uniformly stained.

In addition, intensely DAPI-stained domains were observed. Immunstaining revealed that these domains contained the centromeres and thus represented chromocenters (Fig. 1b, c). Analyses of 200 randomly chosen nuclei revealed that RS nuclei contained four to nine chromocenters (80% of nuclei contained four to six chromocenters) with diameters between 0.45 and 1 μm. Most of these chromocenters (>90%) were aligned at the border between the peripheral DAPI-positive zone and the central chromatin-depleted region. Those chromocenters not localizing at this boundary were associated with the nuclear periphery.

Chicken seems to have a single nucleolus organizer region on michrochromosome 16 (Bloom and Bacon 1985; Delany et al. 2009). Immunostaining revealed that 100% of the nucleoli were aligned along the boundary between the DAPI-positive and DAPI-depleted zones (Fig. 1d, e). Nucleoli were frequently associated with chromocenters. Those parts of nucleoli not in close contact with chromocenters were "exposed" to the DAPI-depleted zone and nucleoli were not surrounded by a layer of chromatin (Fig. 1e).

## The distributions of AT- and GC-rich DNA and of micro- and macrochromosomes

DAPI has a higher affinity for AT-rich DNA (Crissman and Hirons 1994). The fact that the DAPI-depleted zone of RS nuclei showed some staining when PI was applied (Fig. 1f–h), which does not display a higher affinity for specific base pairs, suggested that this central zone contained GC-rich DNA. Furthermore, the relatively low intensity of PI staining in the central zone suggested that chromatin located in this zone was generally strongly decondensed. GC-rich DNA stained by PI but not by DAPI appeared to be enriched around chromocenters (Fig. 1f–h). This implied that GC-rich microchromosomes could be located in these regions.

In order to address the localization of GC-rich and gene-rich microchromosomes (McQueen et al. 1998; Andreozzi et al. 2001; Hillier et al. 2004), and AT-rich macrochromosomes, we performed double-color FISH experiments with a probe hybridizing to most of the microchromosomes and a second probe detecting macrochromosomes 1–5. Figure 2a–l shows two fields of RS nuclei after FISH. In each nucleus, the microchromosomes occupied more central positions, whereas the macrochromosomes occupied more peripheral regions. Chromocenters were not decorated by the probes, which is due to preannealing with Cot-1 DNA. The analysis of fluorescence intensity profiles of single nuclei (Fig. 2m–o) confirmed that microchromosomes occupied more central positions than macrochromosomes and were enriched in the vicinity of chromocenters. These data also confirmed that the central zone in regions not close to chromocenters was generally depleted in DNA (Fig. 2o).

## Nuclear organization of the splicing factor SC35 and of active isoforms of RNA Pol II

As chromatin-depleted regions are often enriched in splicing factors and represent splicing speckles in monolayer cells (Moen et al. 1995; Sadoni et al. 2001), which are associated with GC- and gene-rich DNA (Shopland et al. 2003), we wondered whether the central DNA-depleted zone in RS nuclei might also be enriched in splicing factors. As the essential splicing factor SC35 is typically enriched in splicing speckles, we performed immunostaining of RS with a specific antibody against SC35. The results showed that SC35 was indeed highly enriched in the central DAPI-depleted region and appeared to be mainly restricted to this zone (Fig. 3). Occasional minor focal enrichments of SC35 could also be detected in the more peripheral DAPI-positive zone, but as corresponding cells often displayed a relatively high background staining it was not clear whether such stained foci represented enrichments of SC35 or background staining (immunostaining of tissues often results in higher background than immunostaining of monolayer cells).

Next, we investigated the nuclear localization of active isoforms of RNA Pol II. Two different antibodies were used, which specifically recognize phosphorylation of the C-terminal domain at either serine 2 or at serine 5, respectively. Similar results were obtained with both antibodies (Fig. 4a–f). No staining was observed at chromocenters and at a rim of chromatin at the nuclear periphery. The rest of the

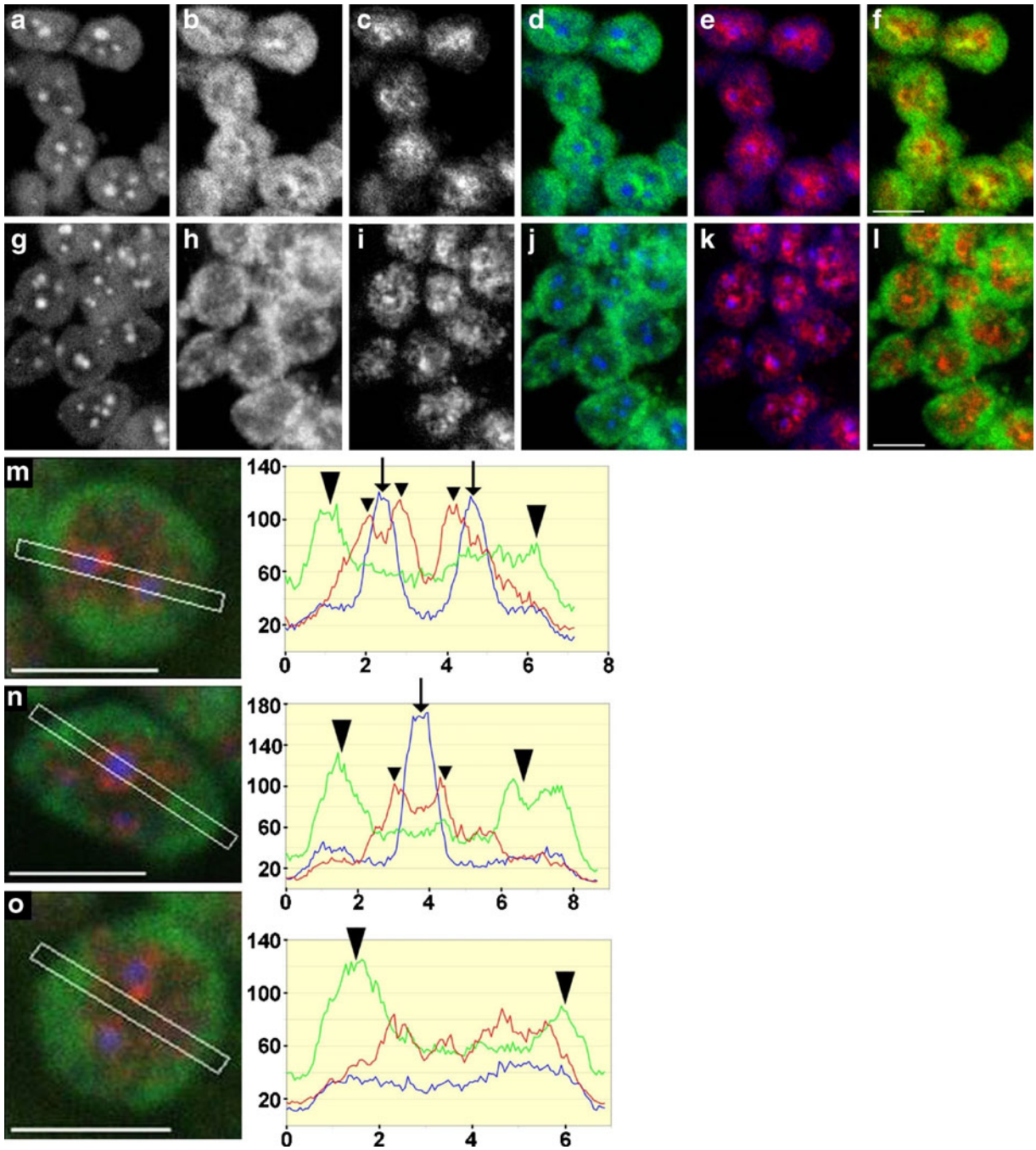


**Fig. 2** Distribution of micro- and macrochromosomes. **a**–**f** and **g**–**l** Show two fields of nuclei after dual-color FISH with probes for macrochromosomes 1–5 (FITC-labeled) and most of the microchromosomes (Cy3-labeled). **a**–**c** and **g**–**i** Show *gray scale* images of the different fluorochromes (DAPI (**a** and **g**), FITC (**b** and **h**), Cy3 (**c** and **i**)). Merges of two colors are shown in **d**–**f** and **j**–**l** (DAPI *blue*, FITC *green*, Cy3 *red*). **m**–**o** Show fluorescence intensity profiles of the regions boxed with white rectangles in the nuclei displayed on the left (macrochromosomes 1–5 *green and green graphs*; microchromosomes *red and red graphs*, DAPI *blue and blue graphs*). The *x*-axes show the lengths of the boxed regions in micrometer (upper left to lower right), whereas the *y*-axes denote the *gray* values of fluorescence intensities. The fluorescence intensity profiles show that the signals of the microchromosomes strongly increase and peak at interior regions (small arrowheads in **m** and **n**) in the vicinity of chromocenters (*arrows*). The signals of the macrochromosomes peak at peripheral regions (*large arrowheads*). **o** Shows a general low concentration of chromosomal DNA in central nuclear regions not close to chromocenters. *Scale bars* 5 μm

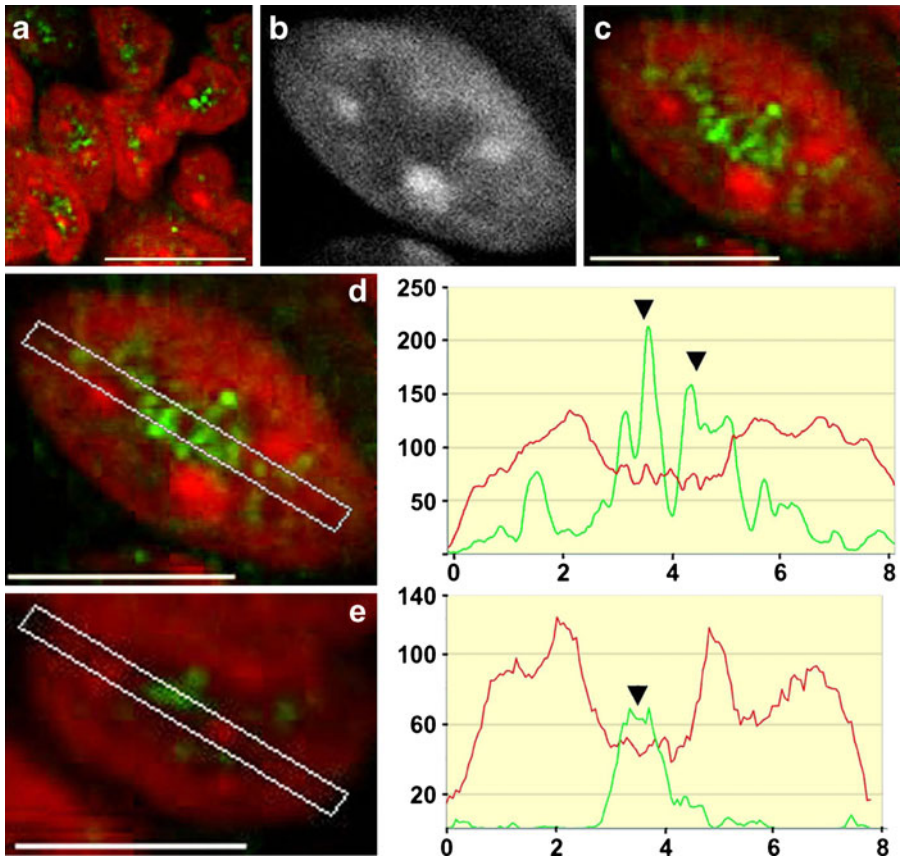


**Fig. 3** SC35 is strongly enriched in the central DAPI-depleted zone. **a** Field of RS nuclei after immunostaining of SC35 (*green*; DAPI *red*). **b**, **c**, and **d** show the same nuclear plane. Only the DAPI staining is displayed in **b**, whereas **c** shows the merge of the SC35 (*green*) and DAPI (*red*) patterns. **d**, **e** Fluorescence intensity profiles of the regions boxed by the white rectangles in the nuclei displayed on the left (SC35 *green and green graph*; DAPI *red and red graph*). The *x*-axis indicates the length of the framed region in micrometer (*upper left to lower right*), while the *y*-axis denotes the *gray values* of fluorescence intensities. SC35-specific fluorescence is strongly enriched in the central DAPI-depleted zone (*arrowheads*). *Scale bars* 5 μm (**c**, **d**, **e**) and 10 μm (**a**)

nuclei displayed intense and slightly granular staining patterns. The peripheral DAPI-positive zones and the central DAPI-depleted zones were stained at about equal intensity. As the chromatin concentration in the central zone is much lower this suggests that the concentration of active RNA Pol II per chromatin unit is much higher in the central DAPI-depleted zone.

## Histone modifications

In mammalian monolayer cells, transcriptionally active regions are enriched in H4K8ac (Sadoni et al. 1999). Immunostaining of RS nuclei with an antibody against H4K8ac resulted in a slightly granular staining pattern (Fig. 4g–i). Also in this case, chromocenters and a rim of chromatin at the nuclear periphery were devoid of staining, but the rest of the nucleus was stained with equal intensity. Thus, the immunostaining patterns of H4K8ac and of the active isoforms of RNA Pol II were similar.

In order to find out where histone modifications typically associated with facultative heterochromatin might reside, we performed immunostaining with antibodies against H3K27me3 and H3K9me2. In both cases, the entire DAPI-positive peripheral zone was labeled, but chromocenters and the DAPI-depleted central zone were not stained (Fig. 5). Together, the results show that specific histone modifications were restricted to defined nuclear zones.

## Different neuronal cell types of RS display a similar form of nuclear architecture

The results showed that the characteristic DAPI staining pattern of RS nuclei highlights structurally and functionally distinct radial zones and is a reliable indicator for the presence of a particular highly ordered form of nuclear organization. During the various experiments, we examined several thousand nuclei of about 200 different RS; and in all cases, the characteristic DAPI staining patterns were observed. This suggested that the corresponding specific form of radial nuclear organization was present in all

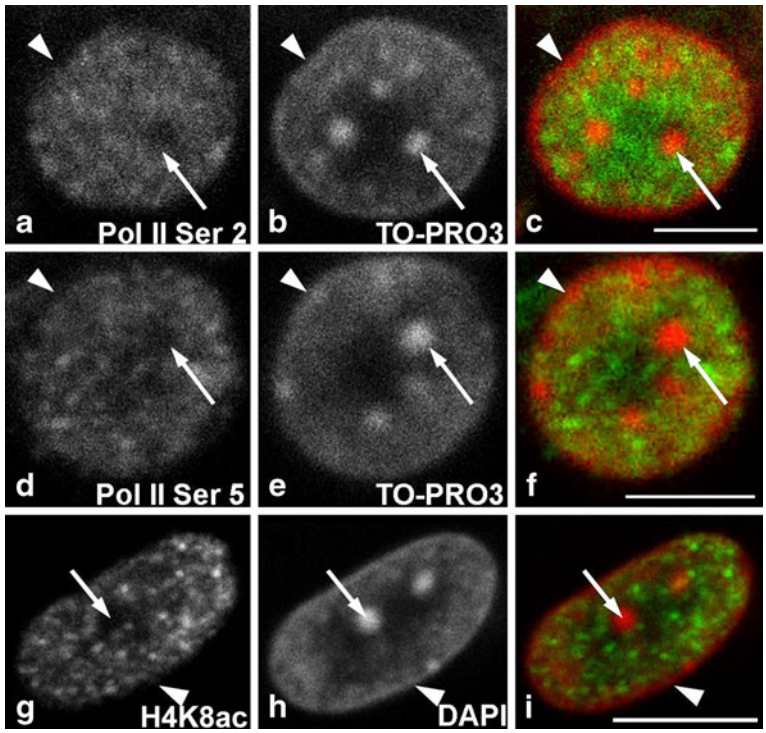


**Fig. 4** Nuclear patterns of active isoforms of RNA Pol II and of H4K8ac. **a**–**f** Immunostaining patterns obtained with two different antibodies against the C-terminal domain of RNA Pol II. One antibody was specific for the active isoform of RNA Pol II phosphorylated at serine 2 (Pol II Ser 2, **a**–**c**), whereas the other antibody specifically recognized phosphorylation at serine 5 (Pol II Ser 5, **d**–**f**). **a** and **d** Show only the immunolabeling patterns, whereas **b** and **e** show the TO-PRO 3 staining of the corresponding nuclear planes. The merges are displayed in **c** and **f** (TO-PRO 3 *red*; immunostaining patterns *green*). **g**–**i** Immunostaining of H4K8ac. The immunstaining pattern **g** as well as the DAPI staining **h** and the merge (**i**, H4K8ac *green*; DAPI *red*) are shown. Chromocenters (*arrows*) and a peripheral rim of chromatin (*arrowheads*) were devoid of immunostaining in all three cases. *Scale bars* 5 μm

different cell types of RS. In order to further address this point, we analyzed nuclear DAPI staining patterns of different RS cell types.

It was examined whether cells displayed a homogenously DAPI-stained peripheral zone and a DAPI-depleted central zone. Furthermore, it was examined whether at least four chromocenters with diameters of at least 0.45 μm were present and whether these chromocenters were aligned along the boundary between a peripheral DAPI-positive and a central DAPI-depleted zone.

First, we identified Müller glia cells by immunostaining of vimentin, which is highly expressed in this cell type. Müller cells stretch out through RS (Fig. S1) and therefore it was difficult to identify their nuclei. Thus, larger numbers of these nuclei could not be examined. Nevertheless, in those cases where it was possible to identify the nucleus of a Müller glia cell the characteristic DAPI staining pattern was observed. Next, we examined amacrine and ganglion cells as well as rods and cones (Fig. 6). For each cell type, 50 nuclei were examined. In each of the 200 nuclei derived from rods, cones, amacrine, and ganglion cells, we observed the highly ordered radial type of nuclear organization as defined by the criteria outlined above. Therefore, this characteristic type of nuclear organization appeared to be specific for neurons and cells of neurogenic capacity (Müller glia cells) but was not specific for particular neuronal cell types.

## RS and neuronal chicken tissues display a similar form of radial nuclear architecture

Next, we examined whether the form of nuclear architecture described above, which is characteristic for chicken neurons in RS, is also present in normal

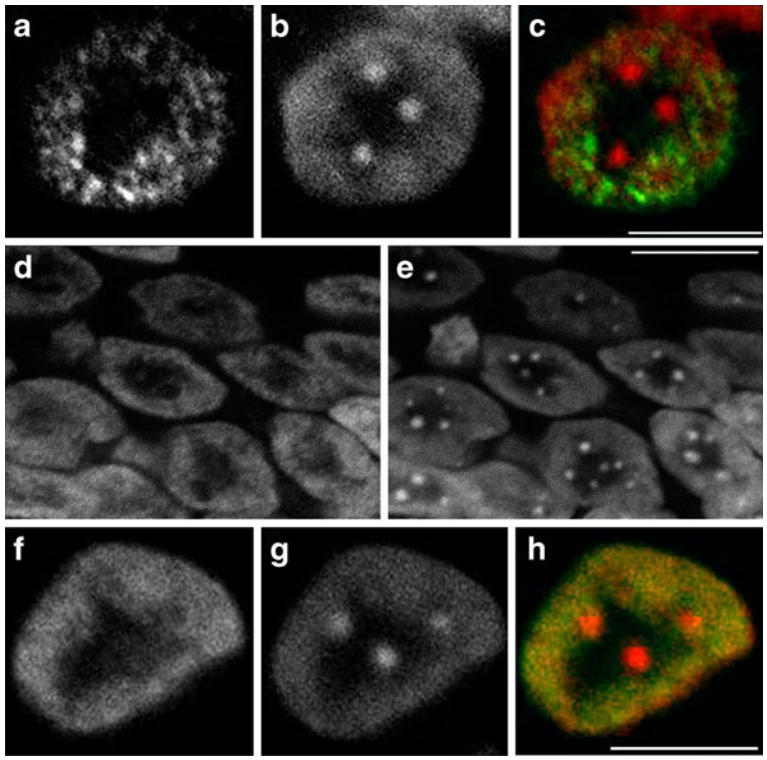


**Fig. 5** H3K27me3 and H3K9me2 are restricted to the peripheral zone in RS nuclei. **a**–**c** Immunostaining of H3K27me3. The immunostaining pattern is shown in **a**, whereas the DAPI staining is displayed in **b**. The merge (DAPI *red*; H3K27me3 *green*) is shown in **c**. **d**–**e** Field of cells immunostained with an antibody against H3K9me2 (immunostaining (**d**); DAPI (**e**)). **f**, **g** Single light optical section of a nucleus after immunostaining of H3K9me2 (immunostaining (**f**), DAPI (**g**)). **h** shows the corresponding merge (DAPI *red*; H3K9me2 *green*). *Scale bar* 5 μm (**a**–**c**, **f**–**h**) and 10 μm (**e**)

chicken neuronal tissues. We examined embryonic brain, dorsal root ganglion, and retina as well as adult brain and spinal cord. In all cases, nuclei displayed the characteristic DAPI staining pattern (peripheral DAPI-positive and central DAPI-depleted zone, chromocenters aligned at the border between these zones, no detectable perinucleolar heterochromatin; Fig. 7). This pattern was not observed in embryonic and adult chicken hepatocytes and myocardial cells or in adult kidney epithelial cells (Fig. 7). These data suggest that the highly ordered form of radial nuclear architecture described here could be specific for chicken neurons in RS and embryonic or adult tissues.

## The nuclear architecture of chicken neurons is remodeled when cells spread on a flat surface

Next, we asked whether the specific form of nuclear architecture present in chicken neurons might be altered when cells spread on a flat substrate. In order to address this question, cells of embryonic chicken retinae (E13) were disaggregated and seeded onto laminin-coated coverslips. Under these conditions, mainly the Müller glia cells spread on the flat surface and form monolayers, while other cell types (mainly photoreceptor cells) attach to the monolayer of Müller cells. These cells do not spread on the 2D surface and form a second layer of cells above the Müller cells.

In order to detect spreading of cells parallel to the 2D surface, we performed immunostaining with an anti-actin antibody. The results showed that those cells closest to the surface of the coverslip displayed the typical spreading as observed in monolayer cultures. A second layer of cells was located above this monolayer, where corresponding spreading was not observed (Fig. 8a, b, d, e). These cells revealed the characteristic DAPI-staining patterns in the nucleus (Fig. 8b; typical numbers and sizes of chromocenters aligned along the

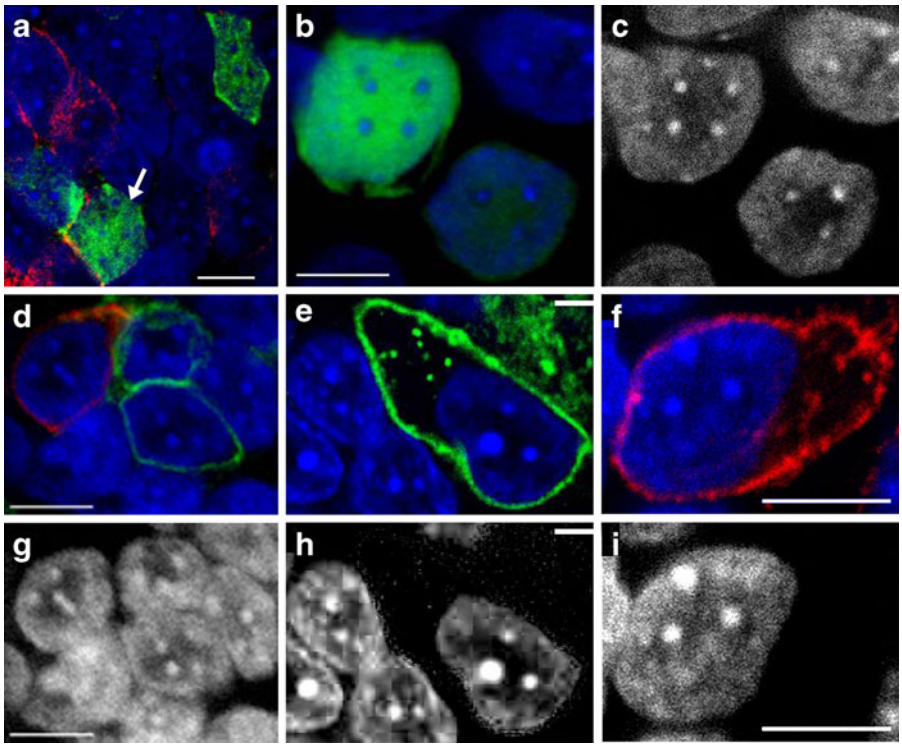


**Fig. 6** Different cell types of RS display a similar nuclear architecture. **a** Field of cells immunostained with antibodies against calretinin (*green*) and acetylcholinesterase (AChE *red*, DAPI *blue*). Calretinin is a marker specific for amacrine cells, whereas AChE is expressed in cholinergic amacrine, ganglion and some horizontal cells. The *arrow* points to a double labeled amacrine cell. **b** Two amacrine cells immunolabeled with the antibody against calretinin (*green*; DAPI *blue*). The lower right cell is only weakly labeled. **c** Shows the corresponding DAPI staining patterns. **d**–**f** Show DAPI (*blue*)-stained nuclei of rod (*red*) and cone (*green*) cells detected by immunostaining with the antibodies Rho4D2 (rods) and CERN906 (cones). **g**–**j** Show only the DAPI staining of the nuclei shown in **d**–**f**. *Scale bars* 5 μm

boundary between a peripheral DAPI-positive and a central DAPI-depleted zone), as also observed in RS in vitro and in neuronal tissues. In contrast, the DAPI-staining patterns of those cells spread on the 2D surface were different. Namely, DAPI-staining patterns were inhomogeneous and nuclei contained several DAPI-depleted regions mixed with more condensed chromatin. In addition, nuclei displayed prominent layers of perinucleolar heterochromatin, which were typically absent in RS nuclei (Fig. 8d, e, g, h).

To find out whether nuclei from other neuronal tissues behaved similarly, dorsal root ganglions were prepared from chicken embryos. Ganglions were kept for 2 days on coverslips in in vitro culture; and during this time period, cells at the bottom attached to and spread on the coverslip. Alternatively, cells from ganglions were dissociated, seeded onto coverslips, and kept for 2 days in in vitro culture. Again, those cells not attached to the substrate displayed the typical neuron-specific form of chromatin organization, while cells spread on the 2D surface displayed a more irregular chromatin organization with several chromatin-depleted areas separated by more condensed chromatin (Fig. 8c, f). Also here, we observed the formation of condensed perinucleolar heterochromatin (Fig. 8i–m), which is typically absent in RS nuclei. Together, these results showed that the nuclear architecture observed in chicken neurons is remodeled when cells spread on a flat substrate.

## Nuclear organization of non-neural chicken monolayer cells

In order to compare the results on nuclear organization described above with the nuclear organization of a chicken cell line cultivated as monolayer we investigated chicken HD12 cells (macrophage cell line, Fig. 9). Prominent chromocenters were not

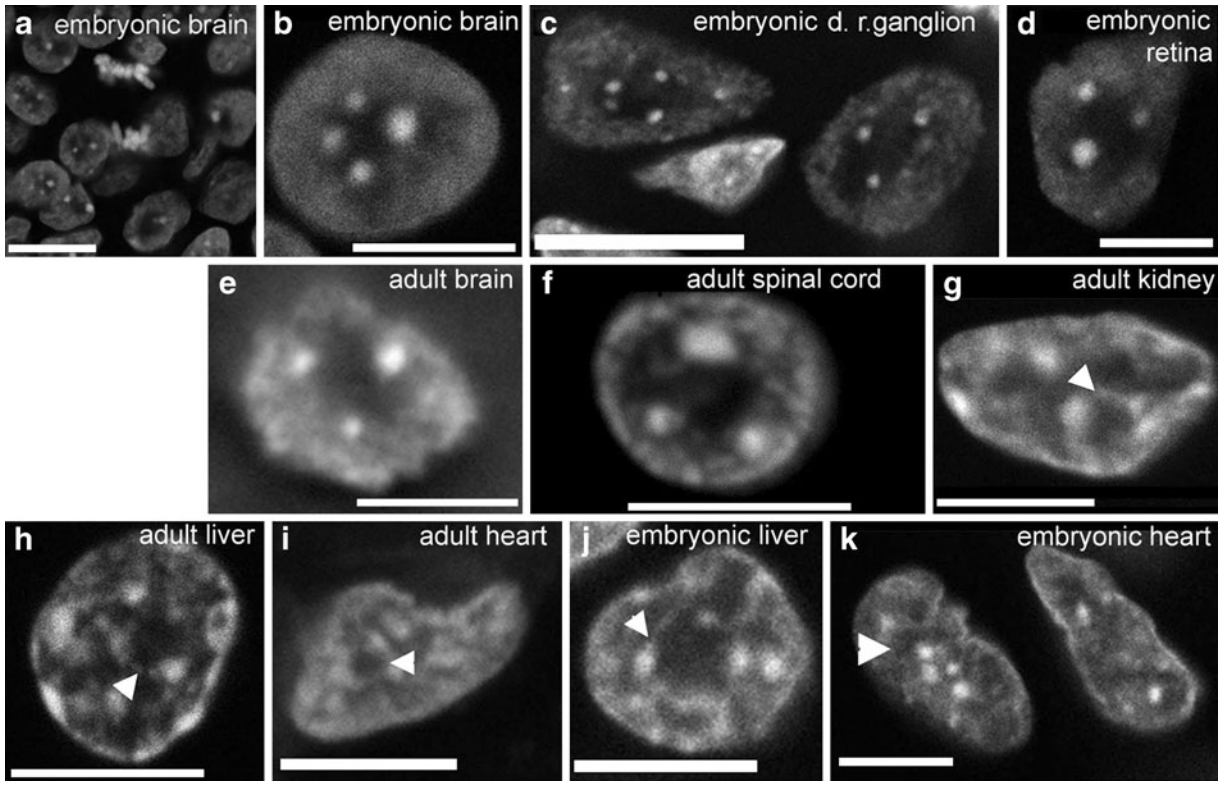


**Fig. 7** DAPI stained nuclei of different chicken tissues. **a**, **b** Embryonic brain (field of nuclei and enlarged nucleus), **c** embryonic dorsal root ganglion, **d** embryonic retina, **e** adult brain, **f** adult spinal cord, **g** adult kidney epithelial cell, **h** adult hepatocyte, **i** adult myocardial cell, **j** embryonic hepatocyte, and **k** embryonic myocardial cells. Perinucleolar heterochromatin (*arrowheads*) is not present in neuronal cell types but is observed in other cell types. *Scale bars* 5 μm (**b**, **d**–**k**) and 10 μm (**a**, **c**)

present in HD12 cells, as revealed by immunostaining of HP1β. Instead, pericentric heterochromatin was distributed over the whole nucleus and many smaller heterochromatic domains intensely stained by DAPI and enriched in HP1β were observed (Fig. 9a and b). In addition, many brightly DAPI-stained domains were observed that were depleted in HP1β. Comparable results were obtained with the chicken DT40 cell line when an antibody against the α isoform of HP1 was used (Gilbert et al. 2003).

Chromatin-depleted areas were scattered over the nuclear interior and were enriched in SC35, which showed the typical speckled pattern of nuclear distribution (Fig. 9c, d). The nucleoli of HD12 cells were embedded into perinucleolar heterochromatin and did not occupy specific nuclear regions (Fig. 9e).

Immunostaining with an antibody against H3K27me3 resulted in only very faint staining of HD12 nuclei (data not shown). Immunostaining with an antibody against H3K9me2 resulted in a focal staining pattern (data not shown). Foci were scattered over the whole nucleus with exception of nucleoli, and no concentration at brightly DAPI-stained chromatin domains could be detected. Similar immunostaining patterns have been observed in human and mouse monolayer cells (Gilbert et al. 2003).

Perinuclear and perinucleolar heterochromatin and other intensely DAPI-stained domains were depleted in H4K8ac (Fig. 9f) and in the active isoform of RNA polymerase II phosphorylated at serine 2 (Pol II Ser 2; Fig. 9g and h). Similar nuclear arrangements of SC35, nucleoli, H4K8ac, and transcriptionally active and heterochromatic domains, as observed here in chicken HD12 cells, have been observed in a great variety of different vertebrate cell types when cultivated as monolayers (see for instance (Moen et al. 1995; Sadoni et al. 1999; Sadoni et al. 2001)).

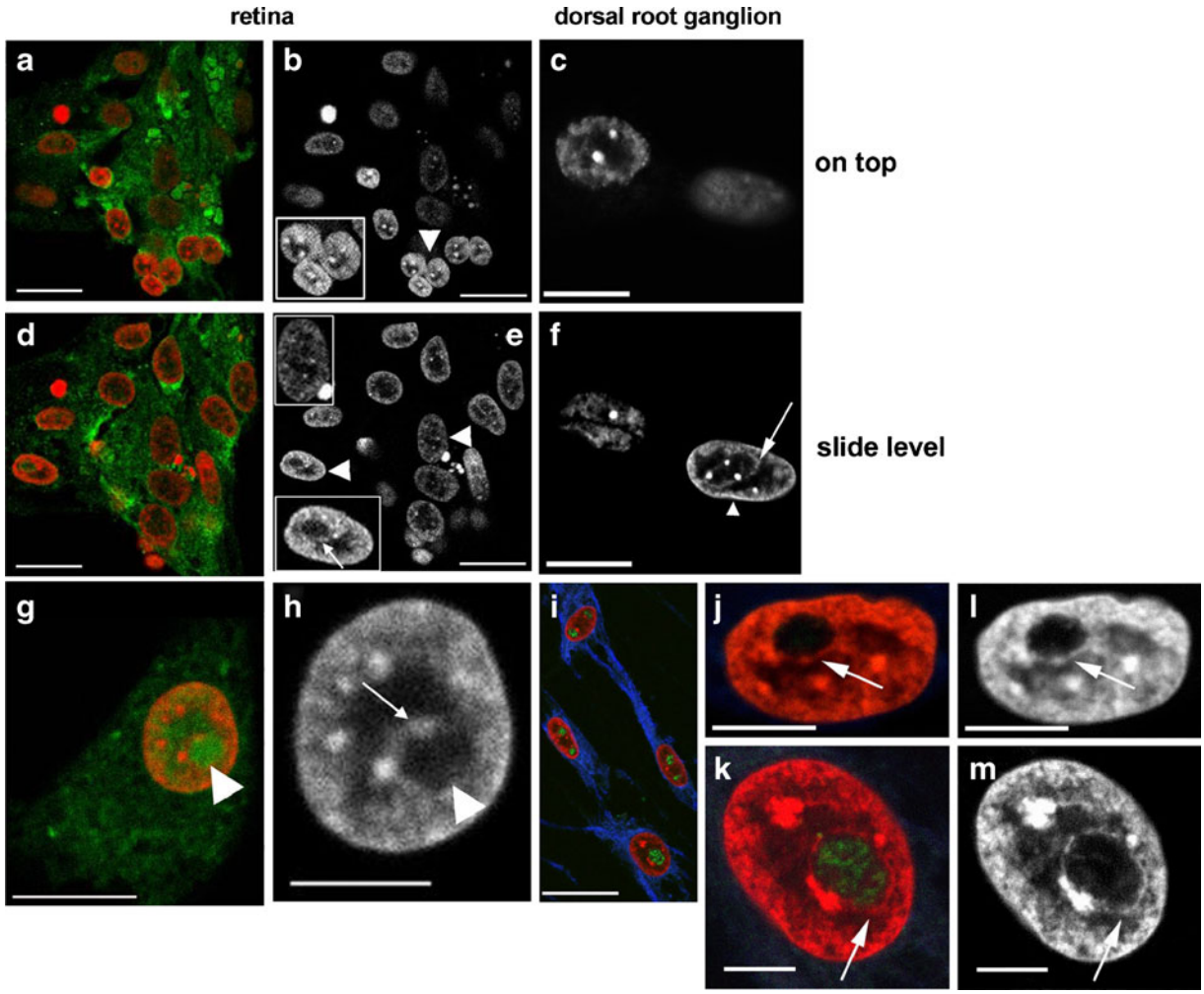


**Fig. 8** Chromatin organization is remodeled in cells spread on a flat surface. Retina **a**, **b**, **d**, **e**, **g**, **h**: cells of an embryonic chicken retina (E13) were disaggregated and seeded onto a laminin-coated coverslip. Spreading of the cytoplasm on the flat surface was visualized by staining with an anti-actin antibody (*green* in **a**, **d**, **g**). **a**, **b** show the same field of cells as panels **d** and **e** (actin *green*; DAPI *red*). Cells localizing in the plane shown in **a**, **b** were on top of the cells shown in **d**, **e** and were not spread on the flat surface. **b** Shows only the corresponding DAPI-staining patterns. The *inset* shows enlargements of three nuclei labeled by an *arrowhead*. Cells in this upper plane displayed the typical nuclear architecture of chicken neurons in a 3D environment (prominent chromocenters at the border between the peripheral DAPI-positive and the central DAPI-depleted zone). **d**, **e** Show cells spread on the flat surface (only DAPI staining shown in **e**). Two cells labeled with *arrowheads* are shown enlarged in the *insets*. Prominent chromocenters are absent and the DAPI staining pattern is inhomogeneous. The nuclear interior is often filled with chromatin and smaller chromatin depleted regions are separated by chromatin bridges (*arrow in the lower inset*). **g**, **h** Another example of a cell spread on the flat surface (actin *green*, DAP: *red*). Immunostaining resulted in some background staining, especially in nucleoli (*arrowhead*). **h** displays in detail the DAPI staining pattern of the nucleus shown in (**g**). The nucleolus (*arrowhead*) is enclosed by a layer of chromatin (*arrow*). *Scale bars* 10 μm (**a**, **b**, **d**, **e**, **g**) and 5 μm (**h**). **c** and **f** Show dissociated cells from a dorsal root ganglion (E12) after 2 days of in vitro culture and the panels show different planes from the same region. Two cells resided in this region and the nuclear DAPI staining patterns are shown. The left-hand cell was not spread on the coverslip and the nucleus displayed the chromatin organization characteristic for chicken neurons in 3D environments. The right-hand cell was spread on the coverslip and its nucleus was elongated and displayed a more irregular chromatin structure with distinct layers of perinuclear (*arrowhead*) and perinucleolar (*arrow*) heterochromatin. **i**–**m** Show cells from ganglions that were kept for 2 days in in vitro culture. The panels show cells from the bottom of the ganglions, which were attached to and spread on the flat surface. Anti-β3 tubulin staining (nerve cell specific) is shown in *blue* and anti-fibrillarin staining is displayed in *green* (DAPI *red*; no anti-fibrillarin staining in panel **j**). **j** and **k** Show enlargements of nuclei from such cells (only the DAPI staining is shown in **l** and **m**). Note irregular chromatin structure and distinct layers of perinucleolar heterochromatin (*arrows*). *Scale bars* 5 μm (**j**, **k**, **l**, **m**), 10 μm (**c**, **f**), and 25 μm (**i**)

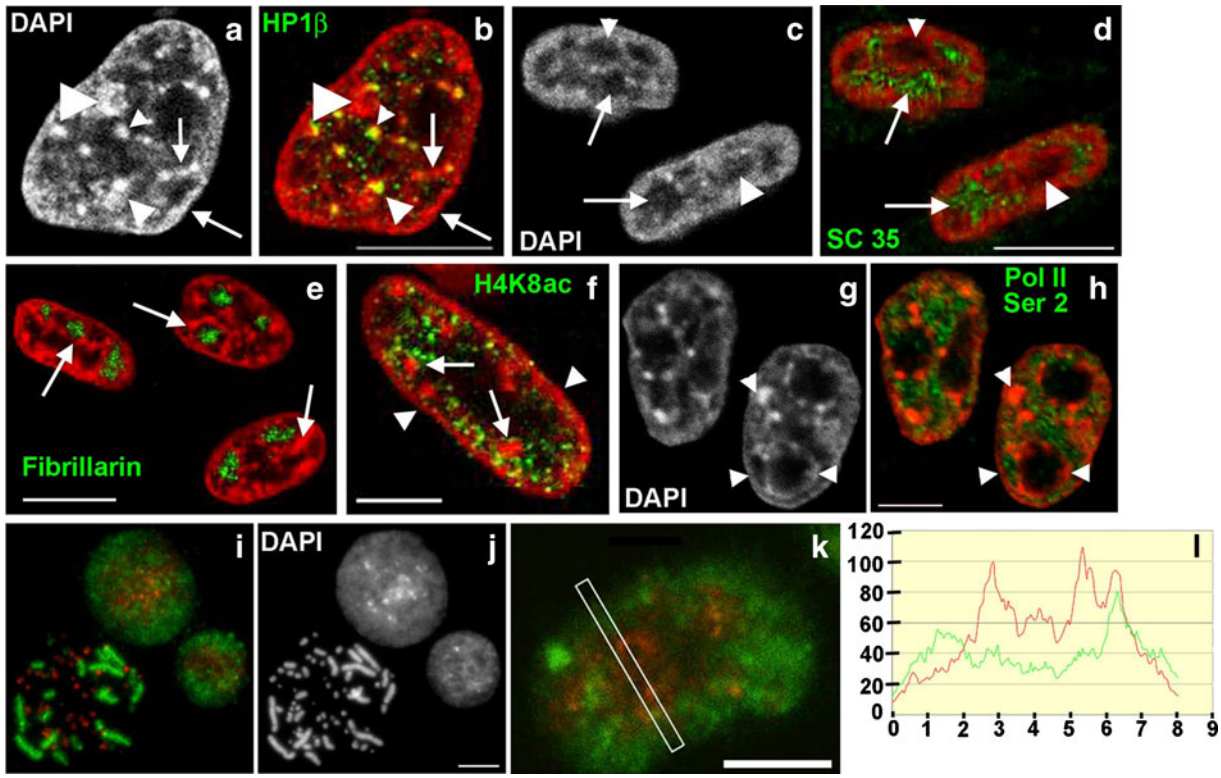


**Fig. 9** Nuclear organization of chicken HD12 monolayer cells. All panels display single light optical sections except **i** and **j** (epifluorescence). **b** Shows immunostaining of HP1β (*green*; DAPI *red*). Only the DAPI staining pattern is shown in **a**. *Small arrowheads* point to heterochromatic domains brightly stained by DAPI and enriched in HP1β. The *large arrowhead* points to condensed chromatin not enriched in HP1β. *Arrows* indicate perinucleolar and perinuclear heterochromatin (not enriched in HP1β). **d** Shows immunostaining of SC35 (*green*; DAPI, *red*). Only the DAPI staining pattern is displayed in **c**. *Arrows* point to splicing speckles, which are enriched in SC35 and depleted in chromatin (*arrowheads* nucleoli). **e** Shows immunostaining of fibrillarin (*green*; DAPI *red*). Nucleoli enriched in fibrillarin are always embedded in intensely DAPI-stained perinucleolar heterochromatin (*arrows*). **f** Shows immunostaining of H4K8ac (*green*; DAPI *red*). Brightly DAPI stained interior heterochromatic domains (*arrows*) and perinuclear heterochromatin (*arrowheads*) are not enriched in H4K8ac. **h** Shows immunostaining of the active form of RNA Pol II (*green*; antibody against phosphorylated serine 2, DAPI *red*). Only the DAPI staining pattern is shown in **g**. Intensely DAPI stained interior heterochromatic domains as well as perinuclear and perinucleolar heterochromatin (*arrowheads*) are devoid of active RNA Pol II. **i** Dual-color FISH with probes specific for macrochromosomes 1–5 (*green*) and microchromosomes (*red*). The panel displays a metaphase chromosome spread and two interphase nuclei. **j** Shows the corresponding DAPI image. **k** Shows a single light optical section of a formaldehyde fixed nucleus after dual-color FISH with the same probes as used in **i**. **l** Displays the fluorescence intensity profile of the region framed by the *white rectangle* in **k** (*red graph* microchromosomes, *green graph* macrochromosomes 1–5). The *x*-axis denotes the length of the framed region in micrometer (from the *upper left* to the *lower right*) and the *y*-axis indicates the *gray values* of fluorescence intensities. *Scale bars* 10 μm (**j**, **b**, **d**) and 5 μm (**k**, **e**, **f**, **h**)

In order to address the patterns of chromosomes in HD12 monolayer cells, dual-color FISH experiments were performed using the probes specific for macrochromosomes 1–5 and for most of the microchromosomes (Fig. 9i and j). The results revealed a radial distribution of micro- and macrochromosomes; microchromosomes preferentially occupied more interior positions compared to macrochromosomes 1–5 (Fig. 9i–l). Thus, also in HD12 cells the most AT-rich and gene-poor parts of the genome preferentially occupy more peripheral positions than the more GC-rich and gene-rich parts. A corresponding radial genome organization has been observed in a large variety of different types of vertebrate monolayer cells (Croft et al. 1999; Sadoni et al. 1999; Boyle et al. 2001; Tanabe et al. 2002; Cremer et al. 2003), and also in embryonic chicken neuronal and fibroblast monolayer cells (Habermann et al. 2001).

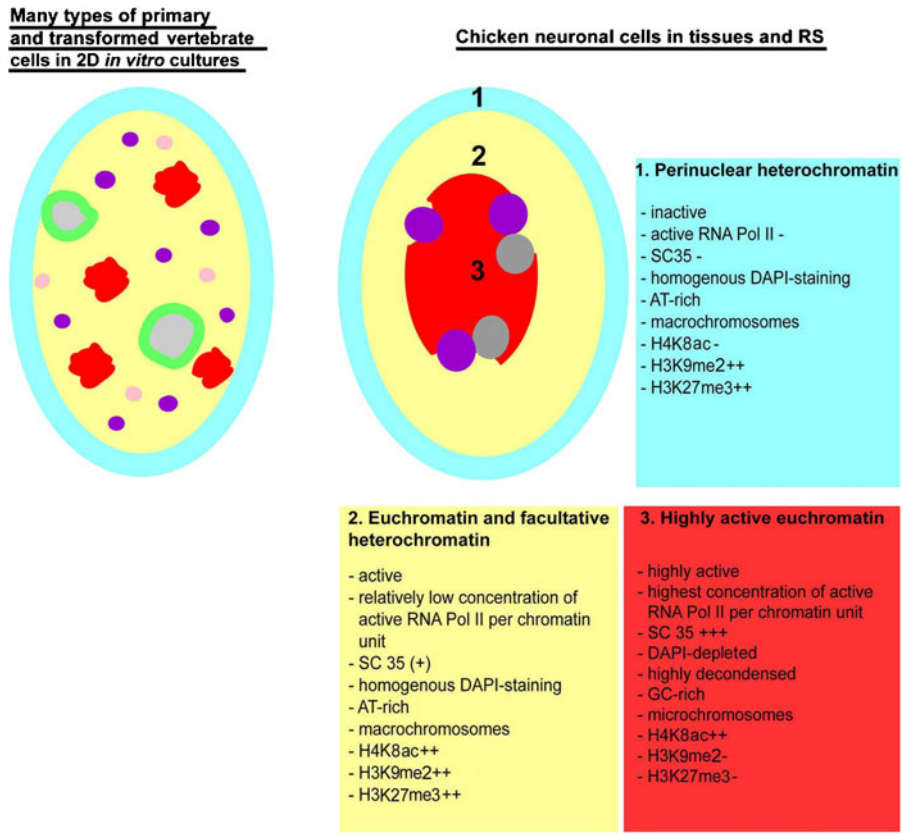


**Fig. 10** The figure illustrates the nuclear organization of chicken and other vertebrate cells in 2D in vitro cultures and the nuclear organization of chicken neurons in tissues and RS. Nuclei of monolayer cells typically contain a layer of perinuclear heterochromatin (*light blue*), which is AT-rich and not enriched in HP1β and H4K8ac. The nuclear interior contains more GC-rich euchromatin (*yellow*) enriched in H4K8ac. The euchromatin is interspersed with condensed heterochromatic domains enriched (*violet*) or not enriched (*pink*) in HP1β and with chromatin depleted regions mainly corresponding to splicing speckles (*red*) and nucleoli (*gray*). Nucleoli usually do not occupy defined nuclear positions and are typically embedded into perinucleolar heterochromatin (*green*). In contrast, nuclei of chicken neurons in a 3D environment are organized into three distinct radial zones (*1*, *2*, *3 light blue*, *yellow*, and *red*). The characteristics of these different zones are listed in the colored fields. Depletion in a specific component is indicated by (−), while (+, ++, and +++) indicate increasing enrichment. Chromocenters (*violet*) and nucleoli (*gray*) align along the border between zones *2* and *3* and are often associated. Nucleoli are not embedded into a shell of perinucleolar heterochromatin but are exposed to the highly active zone *3*

## Discussion

Here, we show that chicken neurons and cells with neurogenic capacity display a highly ordered form of radial nuclear organization when the cells are organized into RS or normal embryonic and adult chicken tissues. It has been shown before that chromosomes and chromatin of vertebrate nuclei display a radial organization (Ferreira et al. 1997; Croft et al. 1999; Sadoni et al. 1999; Boyle et al. 2001; Cremer et al. 2001; Tanabe et al. 2002). This applies also to embryonic chicken neurons and fibroblasts when cultivated on flat substrates (Habermann et al. 2001). However, in the cell types investigated in the previous studies under the conditions applied, the radial organization of chromosomes and chromatin could only be detected after labeling of specific chromosomes or chromatin fractions (e.g., by FISH or replicational pulse labeling) and none of these studies reported that the radial organization was already visible just after DAPI staining.

In the nuclei investigated here, DAPI staining also highlighted the alignment of chromocenters at the border between two radial zones. Non-random

arrangements of chromocenters have been described before (Hsu et al. 1971; Rae and Franke 1972; Manuelidis 1984; Manuelidis 1985; Manuelidis and Borden 1988; Haaf and Schmid 1989; Weierich et al. 2003; Solovei et al. 2004). The chromocenter arrangements described in these studies were different from what has been observed here and to our knowledge ordered radial alignment of chromocenters in the nuclear interior at the boundary between two distinct chromatin fractions has not been reported previously. To our knowledge, no data on chromocenter positioning are available for somatic chicken nuclei. One study investigated the positioning of the centromere of chromosome 1 relative to its chromosome territory (Stadler et al. 2004) but chromocenters or the radial positioning of chromocenters have not been investigated. This applies also to the study by Habermann et al. (2001), which has addressed radial chromosome arrangements in chicken nuclei. It should be noted that the radial form of nuclear organization described here does not only involve chromatin and its different modifications, chromosomes and chromocenters, but also active transcription, nucleoli, and splicing speckles. Together, our data show that chicken neurons in a 3D context display an extreme form of radial nuclear organization that affects simultaneously different chromatin and non-chromatin components and nuclear functions. The findings are summarized in Fig. 10.

To our knowledge, there is only one previous study by Solovei et al. (2009) that reports highly regular radial DAPI staining patterns of vertebrate nuclei, which reveal a radial organization of chromocenters and indicate already the radial arrangement of functionally distinct chromatin fractions. Such patterns were observed in murine rod photoreceptor cells and in photoreceptor cells of other nocturnal mammals. Interestingly, this study (Solovei et al. 2009), which describes an inverted form of radial nuclear organization, has been performed with retinal tissue sections. Thus, this is another example for a special form of radial nuclear organization that has not been identified by using regular cell cultures. Although it is interesting to note that highly regular radial nuclear architectures were observed by Solovei et al. (2009) as well as in our study in rod photoreceptor cells, the types of radial patterns were different (conventional orientation in chicken cells and inverted orientation in murine cells) and we observed the specific form of nuclear organization described here also in other neuronal cell types. The finding that the orientation of the radial organization was conventional in chicken nuclei is in agreement with the results of Solovei et al. (2009), showing that the inverted orientation is only found in nocturnal animals. However, this study was on mammals and did not include birds or other vertebrates. It would be interesting to see whether the association of conventional and inverted orientation with nocturnal or diurnal activity only applies to mammals or includes also non-mammalian vertebrates.

An obvious question is whether the form of nuclear organization characteristic for chicken neurons is also present in other chicken cell types or vertebrates. We have screened non-neuronal embryonic and adult chicken tissues (Fig. 7) and a variety of tissues from other vertebrates (human, gerbil, mouse, rat), including neuronal tissues (data not shown). The tissues were screened after DAPI staining, which highlights the form of nuclear organization typical for chicken neurons. We could not find similar nuclear DAPI staining patterns in non-neuronal chicken tissues or neuronal and non-neuronal tissues of other vertebrates.

Our data show that remodeling of nuclear organization occurs when chicken neurons stretch out on flat substrates. The most obvious change that occurred during nuclear remodeling on flat substrates was the appearance of perinucleolar heterochromatin. Perinucleolar heterochromatin is typically absent in chicken neurons in 3D environments but was frequently observed in chicken neurons on flat substrates. Whether reorganization of the nuclear content was directly due to mechanical forces on cell surface receptors, as described previously (Maniotis et al. 1997), or altered signaling in 2D and 3D environments (Weaver et al. 1997; Cukierman et al. 2001; Bao and Strömblad 2004), is currently unclear. These possibilities are not mutually exclusive.

If nuclear architecture is remodeled when cells spread on flat surfaces, the question is how different tissue-specific forms of nuclear organization are from the nuclear architectures typically observed in monolayer cells. This question is currently difficult to answer as studies on nuclear architecture were mainly focused on monolayer cells. In the future, it would be important to assess the impact of cultivation conditions on nuclear organization. Notably, the highly ordered radial organization of chicken neurons in 3D environments is very different from the nuclear

organization typically observed in monolayer cells (Fig. 10). Primary and transformed monolayer cells from a broad variety of vertebrate species usually display perinucleolar heterochromatin, a speckled distribution of splicing factors, no radial arrangements of nucleoli and chromocenters in the nuclear interior, and radial chromatin arrangements that cannot be visualized by DAPI staining (Fig. 10). Also, chicken HD12 cells in monolayer cultures displayed these features of nuclear organization which are typical for monolayer cells.

Currently, it is not clear why chicken neurons within tissues display a different form of nuclear organization. The control of gene expression and other nuclear functions might play a role. The recent study from Solovei et al. (2009) suggests that rod photoreceptor nuclei act as collecting lenses in the retina of nocturnal mammals. Thus, it appears that nuclear architecture is not always only optimized for the control of nuclear functions, but is also optimized with regard to other cellular functions within the specific tissue context. Further studies on tissue-specific forms of nuclear architecture would be required for a better understanding of the relationships between nuclear architecture and the regulation of nuclear and other cellular functions.

**Acknowledgments** We thank Jeannette Koch (LMU Munich) for artwork and Steffen Dietzel (LMU Munich) for providing HD12 cells. This work was supported by a grant from the Deutsche Forschungsgemeinschaft (La 379/12-5) to PL and by a grant from the VolkswagenStiftung to DZ.

## References

Abbott A (2003) Cell culture: biology's new dimension. Nature 424:870–872

Andreozzi L, Federico C, Motta S et al (2001) Compositional mapping of chicken chromosomes and identification of the gene-richest regions. Chromosome Res 9:521–532

Bao W, Strömblad S (2004) Integrin αv-mediated inactivation of p53 controls a MEK1-dependent melanoma cell survival pathway in three-dimensional collagen. J Cell Biol 167:745–756

Birgersdotter A, Sandberg R, Ernberg I (2005) Gene expression perturbation in vitro—a growing case for three-dimensional (3D) culture systems. Semin Cancer Biol 15:405–412

Bissel MJ, Rizki A, Mian IS (2003) Tissue architecture: the ultimate regulator of breast epithelial function. Curr Opin Cell Biol 15:753–762

Bloom SE, Bacon LD (1985) Linkage of the major histocompatibility (B) complex and the nucleolar organizer region in the chicken: assignment to a michrochromosome. J Hered 76:146–154

Boyle S, Gilchrist S, Bridger JM, Mahy NL, Ellis JA, Bickmore WA (2001) The spatial organization of human chromosomes within the nuclei of normal and emerin-mutant cells. Hum Mol Genet 10:211–219

Chapman RD, Heidemann M, Albert TK et al (2007) Transcribing RNA polymerase II is phosphorylated at CTD residue serine-7. Science 318:1780–1782

Cremer M, von Hase J, Volm T et al (2001) Non-random radial higher-order chromatin arrangements in nuclei of diploid human cells. Chromosome Res 9:541–567

Cremer M, Küpper K, Wagler B et al (2003) Inheritance of gene density-related higher order chromatin arrangements in normal and tumor cell nuclei. J Cell Biol 162:809–820

Crissman HA, Hirons GT (1994) Staining of DNA in live and fixed cells. In: Methods in cell biology. San Diego: Academic Press Inc. pp 195–209

Croft JA, Bridger JM, Boyle S, Perry P, Teague P, Bickmore WA (1999) Differences in the localization and morphology of chromosomes in the human nucleus. J Cell Biol 145:1119–1131

Cukierman E, Pankov R, Stevens DR, Yamada KM (2001) Taking cell–matrix adhesions to the third dimension. Science 294:1708–1712

Delany ME, Robinson CM, Goto RM, Miller MM (2009) Architecture and organization of chicken microchromosome 16: order of the NOR, MHC-Y, and MHC-B subregions. J Hered 100:507–514

Ferreira J, Paolella G, Ramos C, Lamond AI (1997) Spatial organization of large-scale chromatin domains in the nucleus: a magnified view of single chromosome territories. J Cell Biol 139:1597–1610

Ghosh S, Spagnoli GC, Martin I et al (2005) Three-dimensional culture of melanoma cells profoundly affects gene expression profile: a high density oligonucleotide array study. J Cell Physiol 204:522–531

Gilbert N, Boyle S, Sutherland H et al (2003) Formation of facultative heterochromatin in the absence of HP1. EMBO J 22:5540–5550

Haaf T, Schmid M (1989) Centromeric association and non-random distribution of centromeres in human tumour cells. Hum Genet 81:137–143

Habermann FA, Cremer M, Walter J et al (2001) Arrangements of macro- and microchromosomes in chicken cells. Chromosome Res 9:569–584

Hillier LW, Miller W, Birney E et al (2004) Sequence and comparative analysis of the chicken genome provide unique perspectives on vertebrate evolution. Nature 432:695–716

Hsu TC, Cooper JE, Mace ML Jr, Brinkley BR (1971) Arrangement of centromeres in mouse cells. Chromosoma 34:73–87

Jacob V, Rothermel A, Wolf P, Layer PG (2005) Rhodopsin, violet and blue opsin expressions in the chick are highly dependent on tissue and serum conditions. Cells Tissues Organs 180:159–168

Layer PG, Willbold E (1993) Histogenesis of the avian retina in reaggregation culture: from dissociated cells to laminar neuronal networks. Int Rev Cytol 146:1–47

Layer PG, Robitzki A, Rothermel A, Willbold E (2002) Of layers and spheres: the reaggregate approach in tissue engineering. Trends Neurosci 25:131–134

Le Beyec J, Xu R, Lee SY et al (2007) Cell shape regulates global histone acetylation in human mammary epithelial cells. Exp Cell Res 313:3066–3075

Lelievre SA (2009) Contributions of extracellular matrix signaling and tissue architecture to nuclear mechanisms and spatial organization of gene expression control. Biochim Biophys Acta 1790:925–935

Lelievre SA, Weaver VM, Nickerson JA et al (1998) Tissue phenotype depends on reciprocal interactions between the extracellular matrix and the structural organization of the nucleus. Proc Natl Acad Sci USA 95:14711–14716

Maniotis AJ, Chen CS, Ingber DE (1997) Demonstration of mechanical connections between integrins, cytoskeletal filaments, and nucleoplasm that stabilize nuclear structure. Proc Natl Acad Sci USA 94:849–854

Manuelidis L (1984) Different central nervous system cell types display distinct and nonrandom arrangements of satellite DNA sequences. Proc Natl Acad Sci USA 81:3123–3127

Manuelidis L (1985) Indications of centromere movement during interphase and differentiation. Ann NY Acad Sci 450:205–221

Manuelidis L, Borden J (1988) Reproducible compartmentalization of individual chromosome domains in human CNS cells revealed by in situ hybridization and three-dimensional reconstruction. Chromosoma 96:397–410

McQueen HA, Siriaco G, Bird AP (1998) Chicken microchromosomes are hyperacetylated, early replicating, and gene rich. Genome Res 8:621–630

Meaburn KJ, Misteli T (2008) Locus-specific and activity-independent gene repositioning during early tumorigenesis. J Cell Biol 180:39–50

Moen PT Jr, Smith KP, Lawrence JB (1995) Compartmentalization of specific pre-mRNA metabolism: an emerging view. Hum Mol Genet 4 Spec No:1779–1789

Rae PMM, Franke WW (1972) The interphase distribution of satellite DNA-containing heterochromatin in mouse nuclei. Chromosoma 39:443–456

Rothermel A, Layer PG (2001) Photoreceptor plasticity in reaggregates of embryonic chick retina: rods depend on proximal cones and on tissue organization. Eur J Neurosci 13:949–958

Rothermel A, Layer PG (2003) GDNF regulates chicken rod photoreceptor development and survival in reaggregated histotypic retinal spheres. Invest Ophthalmol Vis Sci 44:2221–2228

Rothermel A, Willbold E, Degrip WJ, Layer PG (1997) Pigmented epithelium induces complete retinal reconstitution from dispersed embryonic chick retinae in reaggregation culture. Proc Biol Sci 264:1293–1302

Sadoni N, Langer S, Fauth C et al (1999) Nuclear organization of mammalian genomes: polar chromosome territories build up functionally distinct higher order compartments. J Cell Biol 146:1211–1226

Sadoni N, Sullivan KF, Weinzierl P, Stelzer E, Zink D (2001) Large-scale chromatin fibers of living cells display a discontinous functional organization. Chromosoma 110:39–51

Shopland LS, Johnson CV, Byron M, McNeil J, Lawrence JB (2003) Clustering of multiple specific genes and gene-rich R-bands around SC-35 domains: evidence for local euchromatic neighborhoods. J Cell Biol 162:981–990

Solovei I, Schermelleh L, During K et al (2004) Differences in centromere positioning of cycling and postmitotic human cell types. Chromosoma 112:410–423

Solovei I, Kreysing M, Lanctot C et al (2009) Nuclear architecture of rod photoreceptor cells adapts to vision in mammalian evolution. Cell 137:356–368

Stadler S, Schnapp V, Mayer R et al (2004) The architecture of chicken chromosome territories changes during differentiation. BMC Cell Biol 5:44

Storch K, Eke I, Borgmann K et al (2010) Three-dimensional cell growth confers radioresistance by chromatin density modification. Cancer Res 70:3925–3934

Tanabe H, Habermann FA, Solovei I, Cremer M, Cremer T (2002) Non-random radial arrangements of interphase chromosome territories: evolutionary considerations and functional implications. Mutat Res 504:37–45

Weaver VM, Petersen OW, Wang F et al (1997) Reversion of the malignant phenotype of human breast cells in three-dimensional culture and in vivo by integrin blocking antibodies. J Cell Biol 137:231–245

Weierich C, Brero A, Stein S et al (2003) Three-dimensional arrangements of centromeres and telomeres in nuclei of human and murine lymphocytes. Chromosome Res 11:485–502

Wolf K, Muller R, Borgmann S, Brocker EB, Friedl P (2003) Amoeboid shape change and contact guidance: T-lymphocyte crawling through fibrillar collagen is independent of matrix remodeling by MMPs and other proteases. Blood 102:3262–3269